Source Apportionment and Characterization of Water Insoluble Single Particulate Matters in Rain Sequences Using Particle Size Analyzer and Scanning Electron Microscopy

Ercan BERBERLER

Abant Izzet Baysal Universitesi: Bolu Abant Izzet Baysal Universitesi

Betül Tuba GEMİCİ

Bartin University: Bartin Universitesi

Handan UCUN ÖZEL

Bartin University: Bartin Universitesi

Tuğçe DEMİR

Abant Izzet Baysal Universitesi: Bolu Abant Izzet Baysal Universitesi

Duran KARAKAŞ (✉ dkarakas@ibu.edu.tr)

Bolu Abant İzzet Baysal Üniversitesi: Bolu Abant Izzet Baysal Universitesi

Abstract

In this study, eight independent rainfall events were sampled sequentially from September 20, 2019 to June 15, 2020, in Bartın province located at the western Black Sea coast of Turkey. Manually collected volume based sequential samples were analyzed for pH and water soluble ions involving F^-, Cl^-, NO_3^-, SO_4^{2-}, PO_4^{3-}, Na^+, K^+, NH_4^+, Mg^{2+} and Ca^{2+}. Total trace and major elements (sum of soluble and insoluble fractions), and elemental and organic carbons (EC and OC) contents of the sequential samples were measured. Water insoluble particulate matters in the sequential samples were characterized for their sizes, morphologies and the compositions by using Scanning Electron Microscopy Energy Dispersive X-Ray Spectrometry (SEM-EDS) and particle size analyzer. Results of SEM-EDS, particle size distributions, chemical analyses and the upper atmospheric backtrajectories were used to apportion the sources of the water insoluble single particulate matters in sequential rain samples. Using the proposed method, iron-steel facilities, and thermal power plants were identified as the significant regional sources. Urban traffic and natural emission were identified as the local sources.

Introduction

Sequential rainfall sampling is desirable for obtaining more detailed data relating to the process of pollutant removal from the atmosphere, better evaluating the potential biological and environmental problems, and determining the pollutant source regions and types. It has been known that rainwater is an important sink for atmospheric pollutants and therefore the chemical composition and the amounts of pollutants vary depending on the source regions (Akoto et al. 2011; Bayramoğlu Karşı et al. 2018; White et al. 2013). In sequential rain samples, the amounts of pollutants measured at the earlier sequences of a rain event are significantly higher than the concentrations measured in the following fractional samples of the same rain event. Since the first two or three fractional samples (sequences) are affected by both the rainout (incloud scavenging) and the washout (below-cloud scavenging) processes. On the other hand, the following sequences are affected mainly by the constituents of the rain droplets (rainout) and the regional or local background concentrations at the receptor site. In general, in constant volume based sequential rainfall events, the first and the second sequences remove most of the coarse particulates through washout processes effectively and therefore the following sequences become enriched with fine particulates due to particulate matters (PMs) that are already present in cloud droplets and the additional new fine PMs introduced into sequences by the below cloud scavenging (washout) process. Therefore, the increased number of fine PMs from both rainout and washout processes in a sequential sample can create an opportunity to characterize more single atmospheric particulate matter.

Sequential sampling of rainfall events can be evaluated as one of the useful atmospheric sampling methods to quantify both water soluble and insoluble pollutants and relate them with their possible local and distant sources. However, the presence of secondary air pollutants that are produced through atmospheric chemical and photochemical reactions of gaseous pollutants may sometimes cause complications in source apportionment studies. The rainfall events are stochastic processes and their frequencies of occurrence and depths are random variables that define the temporal structure of the events. On the other hand, the source regions and the source types affecting the air masses during regional atmospheric transports and the aforementioned random variables create more opportunities to detect possible marker species in rain waters. It

is clear that the probability of obtaining single atmospheric particulate matter in sequences of a rainfall event is higher than the samples obtained from direct wet-only deposition, dry deposition, and PM samplings on filter materials. Besides, rain samples represent a column of the atmosphere at the receptor site from ground level to clouds. Therefore, rainwaters naturally involve particles almost in all size fractions which is not the case in PM sampling methodologies in which intended size ranges of PMs are collected. Pollutant amounts in the sequences of rainfall events following the first and the second sequences are less impacted by the earth crust when compared with the ground-level aerosol samplings.

Source apportionment studies require well-characterized and correctly identified, quantified, and speciated pollutant species to obtain reliable results. In addition, examining single atmospheric particulate matter using multiple analytical techniques adds value to source apportionment studies. (J Ding et al. 2019; X Ding et al. 2019). Since working with a single particulate matter can be advantageous for the source identifications and the better understanding of the fates of the particles during atmospheric transports (Xhoffer et al. 1991). Hence, single particle analyses can provide direct evidence for the compositions and the morphologies of the atmospheric PMs (Zeb et al. 2018).

There are several studies in the literature applying Scanning Electron Microscopy Energy Dispersive X-ray Spectroscopy (SEM EDS) directly or as a complementary technique to characterize airborne particulate matters (PMs) in urban atmospheres (Bharti et al. 2017; Karaca et al. 2019; C Y Li et al. 2016; Satsangi & Yadav 2014; Xie et al. 2009; Xue et al. 2019; Yin et al. 2020; Zeb et al. 2018), industrial atmospheres (Yin et al. 2020; Margiotta et al. 2015; Cvetković et al. 2012), rural atmospheres (Wagner et al. 2019; W Li et al. 2020; Delgado et al. 2010). There are several studies using SEM EDS for characterization of the PMs in the samples of raw and treated water (Pivokonsky et al. 2018), marine water (Reisser et al. 2014), snow deposits (Miler & Gosar 2013), fallout PMs in HEPA filtered cleanroom (Malli Mohan et al. 2019), and organic PMs generated by raindrop impaction in soil (Wang et al. 2016). Literature studies show that the Scanning Electron Microscopy (SEM) combined with Energy Dispersive X-Ray Spectrometry (EDS) can be a very useful technique in determining the elemental compositions, sizes, and morphologies of the PMs in a broad range of environmental samples.

To the best of our knowledge, no studies have been conducted to characterize the single atmospheric particulate matter in sequences of a rainfall event using SEM EDS combined with laser diffraction technique directly to determine the particle size distribution in rain sequences without any sample treatment and dispersant introduction.

In this study, we determined the size distributions of water insoluble particulate matters in the sequences of eight independent rain events by using a particle size analyzer directly. For further characterizations of water insoluble PMs for their sizes, chemical compositions, and morphologies we applied several analytical techniques such as ion chromatography for water soluble ions, Inductively Coupled Plasma-Mass Spectrometer (ICP-MS) for the major and trace elements, and SEM EDS for the determination of morphology, size and relative chemical composition or mineralogy of PMs in sequential rainfall samples. However, a complete characterization of PMs requires more sophisticated and expensive instrumentations, such as micro-FTIR, micro-Raman spectroscopy, that should be incorporated into analytical methods (Wagner et al. 2019). For the evaluation and identification of the PMs, we used their relative chemical compositions obtained from SEM EDS and compared the EDS results and SEM images with the literature. Our main goal, in this study, is to show

the advantage of sequential rain sampling in obtaining more single atmospheric PMs per sample compared to ground level wet-only and other PM sampling methods.

Materials And Methods

Sampling sites and sample collection

Eight rainfall events were sampled sequentially using volume based approach from September 20, 2019 to June 15, 2020, in Bartın province located at the western Black Sea coast of Turkey. The first rainfall sample was collected at Bartın University Campus (altitude of 61 m) and the rest of the samples were collected at Orduyeri district of Bartın (41°38'43.5"N and 32°20'03.2"E) approximately 1.0 km far from the city center (**Fig. 1**) at an altitude of 25 m. Manual sequential rain samples were collected by means of a stainless-steel funnel having a 40 cm surface diameter fixed on a stainless steel tripod stand having a height of 1.5 m from the ground level. Samples were collected in prewashed and labeled wide-mouth glass bottles. Volumes of sequences were 200 mL except for the first rainfall event in which the collected sequence volumes were 250 mL.

The long-term (from 1961 to 2020) annual average temperature at the receptor site is 12.8 °C (ranging from 4.0 to 22.0 ºC monthly averages) and the annual average rainfall is 1043.9 mm.

Monthly average rainfall depths change from 54.7 mm (May) to 131.8 mm (December) for the corresponding long-term period (www.mgm.gov.tr). The climate of the sampling region can be categorized as a mesothermal climate with moderate temperatures as a warm-temperate rainy climate. Bartın province, the receptor site, is surrounded by mountains having altitudes lower than 1600 m from north, west, and east sectors and the population of the province was 199,000 as of 2020. Bartın city center is 15 km from the Black Sea and takes place at the eastern sector of the western part of the Black Sea. Sixty-two percent of the region is covered with forests and shrubbery (the forested area is 56 %) and 30 % of the land belongs to agricultural activities. The prevailing wind sectors are north-northeast (16 %), and north and west sectors (7 %). The main sources of air pollution in the province are domestic heating, local traffic, and three highways (755-01, 755-05, and 010-08) around the city and other minor point sources located at the organized industrial zones involving textile (31 %), plastics (18 %), iron and woodworks (13 %). In heating season both coal and natural gas have been used for domestic heating. According to the reports of the Turkish Ministry of Environment and Urbanization, the rate of natural gas usage in the city is 95 % (Environmental Status Report for Bartın City, 2017 and 2019) available in Turkish at https://webdosya.csb.gov.tr/db/ced/icerikler/bart-n_-cdr2017-20181016142716.pdf and https://webdosya.csb.gov.tr/db/ced/icerikler/bart-n_-cdr2019-20201002083843.pdf). However, considering the high levels of PMs (PM_{10} and $PM_{2.5}$) and SO_2 in the heating season, given in the second report, it is understood that a significant amount of coal has still been used for domestic heating. Besides, there are additional potential industrial pollution sources taking place in the neighboring provinces Zonguldak (90 km to Bartın) and Karabük (50 km to Bartın). Zonguldak and the districts, at the west sector of the sampling sites, host Ereğli Iron-steel facility that is one of the biggest iron-steel facilities in Turkey, coal mining facilities, and seven thermal power plants involving the biggest ones in Turkey, namely, Çatalağzı Thermal Power Plant (about 3000 MW). Another potential regional pollutant source for the receptor site in this study is the iron-steel facility in Karabük province located in the south-southeast sector of Bartın.

Sample Analyses

pH measurements of samples and field blank were done at the laboratory, as soon as possible following the sampling, using 15 mL volumes. Following the pH measurements, the sequential samples were divided into varying volumes to be used for further analyses as follow:

100.0 mL of samples were used directly for the particle size distribution using Malvern Mastersizer 3000 (Malvern, UK), having a total of 64 channels or detectors used to measure both the red and the blue parts of measurement, without using any additional dispersant. The analyzer contains a total of 64 channels or detectors used to measure both the red and blue parts of a measurement. In order to prevent the formations of flocculation and/or agglomerations, the samples were subjected to particle size determinations following the pH measurements as soon as possible. Particle size distributions from 0.1 μm to 3.0 mm were determined successfully. In this study, we showed that the particle size distributions in rain sequences can be determined successfully, as reported in our previous work (Bayramoğlu Karşı et al., 2018). One of the most critical steps in this analysis is to purge the sample introduction chamber with ultrapure water (at least two times or more depending on previous samples analyzed) before the sample introduction due to low PM contents in the sequences. Another important point in this measurement is the sample volume to be used for the particle size distributions. Rain sequence samples contain limited amounts of particulate matter, therefore, at least 100.0 mL of sample is required for the analyzer used.

 50.0 mL of the samples were transferred into HDPE bottles and acidified with supra pure nitric acid and stored at +4 ^oC until ICP-MS analyses for total (soluble and insoluble) major and trace metals including Ag, Al, As, Ba, Be, Bi, Cd, Co, Cr, Cs, Cu, Fe, Ga, Li, Mg, Mn, Mo, Ni, Pb, Sb, Se, Sn, Sr, Tl, V, and Zn. For the digestions of sequential samples Method 3005A (US EPA) was followed with some partial modifications. Briefly, the samples were transferred into clean beakers and 5 mL of concentrated nitric acid (Merck Supra Pure, Germany), 1 mL of concentrated hydrochloric acid (Merck Supra Pure, Germany), and 1 mL of concentrated hydrofluoric acid (Merck Pro analysis, Germany) were added. The beakers were covered with watch glasses and placed in a water bath at 80 ± 5 ^oC. The samples were evaporated without boiling to volumes of about 2-3 mL and the same amounts of acids were added once more and re-evaporated to final volumes of about 2 mL. The pre-concentrated samples were transferred into Teflon vessels, 5 mL nitric acid, 1 mL hydrochloric acid, and 0.5 mL hydrofluoric acid were added and the samples were digested using ETHOS One Microwave Digestion System (Milestone Inc., USA) for 15 and 20 min. hold times at 175 ^oC and 200 ^oC, respectively.   After digestion, the samples were diluted to 15 mL final volumes without filtration. Total recoverable metals were determined by using Elan DRC-e ICP MS (Perkin Elmer SCIEX, Norwalk, CT USA). EnviroMAT-Drinking water-Low SRM (SCP SCIENCE, Quebec, Canada) was used to test the metal recoveries.

25.0 mL of samples were filtered through cellulose acetate filters having a pore size of 0.22 μm, following the pH measurements, for the determinations of water soluble anions (F^-, Cl^-, NO_2^-, NO_3^-, PO_4^{3-}, and SO_4^{2-}) and cations (Li^+, Na^+, NH_4^+, K^+, Mg^{2+}, and Ca^{2+}) using Dionex ICS-1100 model ion chromatography equipped with a conductivity detector and AS-DV autosampler. Analyses of samples for water soluble ions were performed the day after sampling. The cellulose acetate filters used to filter the samples for ion chromatography were transferred into acid-washed glass Petri dishes, labeled, and dried overnight at low temperatures (35-40 ^oC). Samples of about 12 mm^2 from the filters were cut under a laminar flow clean cabinet equipped with a HEPA

filter unit and a homemade charcoal cartridge preceding the HEPA filter. Finally, samples were sealed, re-labeled, and transferred to the Central Laboratory of Bartın University to carry out the SEM-EDS analyses. Before SEM-EDS analyses, the samples were coated with Palladium (Pd) and Gold (Au) mixture (about 10 nm thick). Then the samples were transferred to the SEM (TESCAN, MAIA3 XMU model, Czech Republic) for the PM characterization.

The remaining volumes (about 10.0 mL) of the samples in glass bottles were stored at +4 $^{\circ}$C to determine the elemental carbon (EC) and organic carbon (OC) contents of the sequential samples. From each sample, 10 successive 100 μL aliquots were added onto a 1.5 cm^2 punch of a pre-fired (at 900 $^{\circ}$C for 4 hours) quartz fiber filter. After each addition, the filter punch was dried at room temperature in a laminar flow clean cabinet. Finally, the filter punches containing residues from a total of 1.0 mL sample were analyzed for OC and EC using desktop thermal-optical Sunset OC/EC Analyzer (Sunset Laboratory, Oregon, USA) using NIOSH 870 protocol (Birch and Cary, 1996). Method recovery for OC was tested using NIST SRM 1648a, Urban Dust, and determined as 98.0 ± 7.2 %. The method detection limit was calculated as 0.15 μg C/mL rainwater. For the method detection limit calculation, we used results of 10 replicate measurements of pre-fired quartz filters. The standard deviation of replicate results was multiplied by 3 and then by 1.5 (punch area) and divided by 1.0 mL. The field blank levels of EC were lower than the method detection limit, however, detectable amounts of OC were measured in the field blanks and used for the correction of particulate OC results.

Results And Discussions

Rainfall events

Hourly meteorological data corresponding to sampling time intervals was obtained from the meteorology station located at the city center of Bartın (Station code: 17020). Upper atmospheric backward trajectories for the corresponding rain events were calculated from the Hybrid Single-Particle Lagrangian Integrated Trajectory (HYSPLIT) modeling system (Rolph et al, 2017; Stein et al, 2015). The isentropic HYSPLIT model was run to compute 120 h backward trajectories for 500, 1000, and 1500 m above ground level (AGL) to account for the maximum fractions of the boundary layer, and GFS (0.25°, global) was selected as meteorology input data.

Sampling times and the antecedent dry days prior to sampling each rainfall event were given in **Table 1**. Sample information including sampling date, number of sequences and acidic sequences (pH < 5.6), mean pH of sequences, and the mean ratio of the sum of anions to the sum of cations (the equivalent ratio) for each of the rain events were presented in **Table 2**.

Table 1. Sampling times and antecedent dry days

Rainfall event	Date	Start time (UTC)	End time (UTC)	No of antecedent dry days
1	September 20, 2019	11:58	20:01	> 20
2	October 08, 2019	04:50	14:22	2.0
3	November 30, 2019	18:24	19:25	1.0
4	November 30, 2019 – December 01, 2019	20:03	01:04	0.03
5	February 03-04, 2020	17:10	0:00	2.0
6	May 04, 2020	10:56	17:15	0.17
7	May 29, 2020	03:26	12:07	0.12
8	June 15, 2020	09:11	13:40	0.25

The abundances of atmospheric PMs depend on the number of antecedent dry days which means that as the number of dry days increase, the amounts of PMs in the atmosphere increase. Therefore, the water qualities of rainfall events (events 1, 2, 3, and 5 in this study) following dry days were affected mainly by the washout mechanisms, whereas the rainout mechanism became more dominant in rainwater composition (event numbers 4, 6, 7, and 8) (Table 1) due to prewashed air mass column below cloud levels.

Table 2. Samples information

Rainfall event	Date	No of sequences	Acidic sequences	pH	Σanion[b]	Σcation[b]	Σanion/ Σcation
1	September 20, 2019	4	All	4.9 ± 0.32	47.4 ± 30.1	59.4 ± 35.2	0.82 ± 0.16
2	October 08, 2019	5	None	5.88 ± 0.28	46.4 ± 38.4	46.0 ± 41.8	1.06 ± 0.12
3	November 30, 2019	4	None	6.35 ± 0.21	80.4 ± 76.6	98.3 ± 80.2	0.93 ± 0.37
4	November 30, 2019 – December 01, 2019	5	1st	5.78 ± 0.33	25.9 ± 9.19	33.6 ± 23.0	0.88 ± 0.23
5	February 03-04, 2020	10	2nd and 3rd	5.90 ± 0.33	108 ± 80.3	139 ± 120	0.88 ± 0.32
6	May 04, 2020	6	None	5.97 ± 0.29	26.1 ± 2.32	36.7 ± 6.41	0.73 ± 0.21[a]
7	May 29, 2020	12	None	6.10 ± 0.24	28.3 ± 5.36	33.4 ± 6.76	0.87 ± 0.22[a]
8	June 15, 2020	14	1st and 2nd	6.08 ± 0.44	10.9 ± 6.28	12.5 ± 6.87	0.89 ± 0.21

[a]Ratio includes bicarbonate (HCO_3^-) which was calculated based on measured pH values (Anatolaki & Tsitouridou 2009).

[b]Σanion and Σcation are the mean equivalences of total anions and cations calculated from sequential samples.

The equivalent ratios of total anions to total cations have been used to check the completeness of the measured ions and analytical data quality. When the equivalent ratio of total anions to total cations is within the interval of 1.0 ± 0.25 then the data is commonly assumed acceptable (Anil et al., 2019). The mean equivalent ratios of the total anions to total cations in this study (Table 2) changed from 0.82 ± 0.16 (event 1) to 1.06 ± 0.12 (event 2) for all the rainfall events, except for the events 6 and 7. The mean anion to cation ratios for these events was calculated as 0.38 ± 0.21 and 0.30 ± 0.13, respectively. In this case, there is a significant level of anion deficiency that cannot be attributed to unmeasured organic anions. In order to check the completeness of the measured ions, we added calculated equivalent values of bicarbonate to the equivalents of total anions. After adding bicarbonates, the equivalent ratios of total anions to total cations become 0.73 ± 0.21 and 0.87 ± 0.22, as presented in **Table 2**. As discussed below the samples of events 6 and 7 contained high levels of calcium ion and therefore, the anion deficiency in these samples can be clearly attributed to bicarbonate ion as also discussed in Section 3.4. The lowest total ion concentrations were observed in the samples of rainfall events 1 and 4. Rainfall events without acidic sequences, namely, rainfall events 2, 6, and 7

had the highest calcium ion concentrations, 15.1 µg/mL, 28.1 µg/mL, and 17.2 µg/mL, respectively (**Table S1**). The third rainfall event did not have an acidic sequence even having similar levels of nitrate and sulfate (5.1 and 5.7 µg/mL, respectively) concentrations with the events 2, 6, and 7. Besides, the ammonium and the calcium ions, main neutralizing agents, concentrations are 10 to 18 times, and 5 to 11 times, respectively, lower than the concentrations measured in the samples of rainfall events 2 and 6. However, the third event samples contained higher levels of chloride (12.9 and 6.5 times higher than the concentrations observed for events 2 and 6) and sodium (4.7 and 7.7 times higher than that of levels observed in the samples of events 2 and 6) ions which show that the rainfall event 3 had been affected mainly by Mediterranean and Aegean Sea when the low levels of anthropogenic pollutants and the 1500 m backtrajectory path following the western region of Turkey were considered. Among the eight rainfall events, the fifth rainfall event was the most polluted one having the highest concentrations of chloride (9.4 µg/mL), nitrate (15.5 µg/mL; 2.6 to 11 times higher than the others), sulfate (25.4 µg/mL; 4.4 to 12 times higher), ammonium ion (4.75 µg/mL; 2.2 to 40 times higher than the maximum and the minimum levels observed among the others). Sodium (8.74 µg/mL) and calcium (12.4 µg/mL) ions levels were also observed at higher levels. As will be discussed in the following sections, the air masses of the fifth rainfall event follow the path over the most industrialized region of Turkey (Marmara region) and the zone of industrial activities including iron-steel and power plant facilities (**Fig. S4 (a)**).

Air mass backtrajectory results showed that all the air masses, except for the rainfall events 3, 7, and 8, pass over Zonguldak province hosting the main point sources like iron-steel and power plants. On the other hand, the upper atmospheric air masses (1000 and 1500 m) corresponding to rainfall event 5 follow the path from the Black Sea to the sampling site while the 500 m component follow a slightly different path in which, after reaching the coastal site, it sinks down and pass over Zonguldak region before precipitation. Air masses of rainfall event 8 (**Fig. S4 (b)**) come directly from the west however, the corresponding air masses spent about 70 % of their total residence times at ground levels at the zone where Karabük Iron-steel Facility takes place. Therefore, as will be discussed in SEM results section, the observed PMs must represent the characteristics of emissions from forests and Karabük Iron-steel Facility.

pH distributions

The mean pH of the four sequences of the first rainfall event was determined as 4.9 ± 0.32 and changed between 4.5 and 5.2 which showed that all the sequential sub-samples are in acidic character (pH < 5.6) (**Table 2**). The local wind rose and the upper atmospheric air masses at 500 and 1000 m enters the sampling site from N-NE sector (**Figure 2**). However, 1500 m above ground level (AGL) air mass (the green line) spends almost all its time (5 days) at the coastal line between Sakarya and Samsun provinces which covers one of the most industrialized regions of Turkey. The main pollutant sources in this coastal site are Ereğli Iron-steel Facility, Zonguldak province itself, and its districts hosting seven thermal power plants including Çatalağzı Thermal Power Plant facility. The wind directions reported for Bartın may not represent the correct wind sector due to geographical structure which causes wind re-circulation events. However, whatever the situation is, the local wind direction shows that the first rain event was also contributed by the urban atmosphere of Bartın province.

Therefore, the 1500 m air mass and local wind rose to show that the first rain event was affected significantly by iron-steel work facilities, thermal power plants, and the urban atmosphere of Bartın province hence resulted

in acidic rain waters. On the other hand, it is difficult to differentiate between the sources of free acidity due to additional contributions made by the organic acids found in the atmosphere as reported by Rosa M Peña et al. (2002) for the northwest region of Spain. It was reported that the most frequently observed acids in rain waters are formic and acetic acids followed by oxalic, lactic, and citric acids (Peña et al. 2002). Organic acids may have contributed to the free acidity since the sampling site, in this study, is a forested area and under the influence of both urban and industrial atmospheres. This effect can also be clearly seen from the equivalent ratios of total anions and total cations as discussed above. Except for the second rainfall event, there are 7 to 17% of anion deficiencies in the samples that can be attributed to contributions due to the organic acids. None of the fractions corresponding to rainfall events of 2, 3, 6, and 7 showed an acidic rain character. However, the first fraction of the rainfall event 4, the second and the third fractions of rainfall event 5, and the first and the second fractions of rainfall event 8 showed acidic characters due to very short antecedent dry periods, that is, the main neutralizing agents like calcium, carbonates, and ammonia were washed out from the atmosphere by the preceding rain events.

Ions, trace and major elements

Non-sea salt concentrations of water soluble ions were used in this paper and sodium ion concentration was used as a reference ion for sea salt to calculate the non-sea salt fractions. Both anions and cations showed negative correlations with the rain intensities. This relation explains the concentration increases at the last sequences of a rainfall event which is the general observation in sequential rain samplings. Sum of equivalences of anions to the sum of equivalences of cations ratio of all rainfall events changed at acceptable levels, except for the rain events 6 and 7 (Table 2). In general, except for the second event, anion deficiencies were observed for all of the rainfall events that can be attributed to unmeasured bicarbonate ions (Bayramoğlu Karşı et al. 2018). However, the observed anion deficiencies in the sixth and the seventh rainfall events were very significant and they cannot be explained by the absence of bicarbonate. Therefore, the anion deficiencies observed for these two samples can be attributed to other unmeasured anions originating from biological and anthropogenic organic acids. Phosphate ion concentration was below the detection limit in all the samples. Statistically significant correlations between anions and the cations related to the agricultural activities show that the washout mechanism is much more effective than the rainout mechanism. This observation supports the dominancy of local pollution sources rather than the long-range transport of pollutants which is represented by the rainout process. The ion pairs that showed significant correlation coefficients (95 % CL, p < 0.05) are; NH_4^+ and K^+ (0.82), NO_3^- and SO_4^{-2} (0.69), NH_4^+ and NO_3^- (0.96), K^+ and NO_3^- (0.84), K^+ and SO_4^{-2} (0.87). The correlation coefficient between the sulfate and ammonium ions was not significant (around 0.40) which shows that there was no significant amount of ammonium sulfate in the samples. The presence of ammonium sulfate in the atmospheric samples has been used as an indicator for the aged particles, therefore, the result observed in this study supports the effectiveness of the local sources. The relative contribution of the washout process on the non-sea salt water soluble ions were calculated using the approach in our previous publication (Bayramoğlu Karşı et al. 2018). The results were presented in Table 3.

Table 3. Relative amounts of non-sea salt water soluble ions scavenged by washout process (%)

ID	Ammonium	Potassium	Magnesium	Calcium	Floride	Chloride	Nitrate	Sulfate
Rainfall-1	65.1	42.2	63.7	82.1	nd	41.5	71.2	88.9
Rainfall-2	81.7	46.5	95.9	99.2	78.4	69.7	84.9	79.6
Rainfall-3	94.3	59.5	98.0	99.0	nd	72.5	88.4	88.3
Rainfall-4	nd	26.5	nd	97.7	nd	90.6	67.2	69.4
Rainfall-5	96.8	84.8	94.4	98.6	95.5	nd	96.3	95.7
Rainfall-6	99.9	69.8	98.6	98.4	nd	84.7	94.9	82.2
Rainfall-7	98.2	90.5	98.0	97.9	nd	91.7	92.8	97.8
Rainfall-8	98.8	92.6	66.4	96.5	95.5	88.2	98.1	97.4

nd: Not detected.

The relative amounts of ions presented in **Table 3** can be evaluated as local contributions to the total ionic compositions. On the other hand, the rainout mechanism or long-range transport represents the amounts of pollutants transported to the receptor site by both cloud droplets and the corresponding upper atmospheric air masses. The relative amount of rainout contribution can be calculated simply by subtracting the values in **Table 3** from 100 for each of the ions. The calculated relative amounts of ions for the rainout process may be considered as approximate values since there are always local and/or regional background concentrations at the below cloud levels. For this reason, as will be discussed below, similar types of PMs are frequently observed in almost all of the sequential samples. The most significant contributions made by the rainout mechanism are very clear in the results of the first and the fourth rainfall events (**Table 3**), except for calcium and sulfate in the first event and again calcium and chloride in the second event. Potassium ions had the highest rainout to washout ratio among the samples (except for the samples of 5th, 7th and 8th rainfall events) and followed by the chloride. It is clear that all the ions from the rainfall events 5, 6, 7, and 8 show the lowest rainout to washout ratios (20 % or less) compared to the previous four rainfall events which showed varying ratios depending on the specific ions, like potassium, chloride, ammonium, and magnesium. In conclusion, the washout mechanism was observed to be a more effective factor in the scavenging of water soluble ions than the incloud scavenging (rainout) mechanism.

The concentrations of trace and major elements (sum of dissolved and insoluble fractions) measured in this study were presented in **Table S2** for the rainfall events 4, 5, 6, and 7. Among the four rainfall events, the fifth rainfall event was the most polluted one with respect to measured elements as in the case of water soluble ions. Backtrajectory results show that the air masses of the fifth rainfall event follow the path over the most industrialized region of Turkey and the zone of industrial activities including iron-steel and power plant facilities (**Fig. S4 (a)**). Aluminum concentration in the fifth rainfall event sample was 2 times higher than the

concentrations measured in the samples of the fourth and the sixth events, and 35 times higher than the concentration measured in the sample of the seventh event. Again the As concentration in the fifth rainfall event sample was 1.3, 3.0, and 5.0 times higher than the concentrations measured in the samples of rainfall events 4, 6, and 7, respectively. Both crustal and industrial elements had the highest concentrations in the fifth rainfall event compared to the other three rainfall events. The elements, namely, Sb, Sn, and V had almost similar concentrations in the samples of fourth and fifth rainfall event samples. Rainfall event 7 samples was observed to be the least polluted one except for the elements Ba, Bi, Cu, Cs, Pb, and Zn which are higher than or at comparable levels with the other rainfall event samples. Backtrajectory results showed that the 500, 1000, and 1500 m air masses originate in Poland and pass over Ukraine, Moldova, and the Black Sea before reaching the sampling site. Air mass of 500 m corresponding to the seventh rainfall event sinks down on the Blacks Sea coast for about 12.6 hours and then rises back to 500 m altitude in about 6.3 hours before precipitation. Therefore, backtrajectory results confirmed that the air masses of the seventh rainfall event were not affected by the industrial sources taking place in the sampling region. The lowest and the highest levels of Mg, Al, Fe, Li Sn, and V were observed in the samples of rainfall events 7 and 5, respectively (**Table S2**).

Major and trace elements concentrations showed different behaviors with the rain intensities compared with the water soluble ions. In this study, the observed mathematical relations between the elements and the rain intensity were not similar among the elements measured and differed from one rainfall event to another. This is an expected result since the emission sources, and therefore, pollutant characteristics are not similar for the independent rainfall events. Both negative and positive coefficients (i.e. inversely or directly proportional) were observed in the first terms of the fitted model equations explaining the relations between the elemental concentrations and the rain intensities among the rainfall events. The elements having a linear relationship with the rain intensity are Al, Ba, Ga, Mg, Mn, and V. The metals like Co, Cs, Fe, Li, Pb, and Sn showed linear or quadratic relationships with the rain intensity among the events. However, the elements, namely, As, Bi, Cd, Cr, Cu, Mo, Ni, Sb, Se, Sr, and Zn showed quadratic relationships with the rain intensities in all of the rainfall samples. These results show that the below cloud scavenging of elements is affected by three main factors: (1) impaction of rain droplet to the PM, (2) PM size, and (3) the solubility of PM or its chemical components in water (Bayramoğlu Karşı et al. 2018; Lim et al. 1991). Therefore, due to the inefficacy of the washout mechanism in scavenging of PM, the concentrations of elements did not show decreasing trend with increasing sequence numbers, unlike water soluble ions, due to limited solubilities of metal oxides and salts. Therefore, the concentration contributions from rainout and washout mechanisms to the scavenging of metals cannot be discriminated easily.

Organic and elemental carbons

The mean and the total concentrations of particulate organic carbons (OC) and elemental carbons (EC) for each rainfall event are given in **Table 4**. Mean values represent the average concentrations calculated from the sequences having equal volumes, therefore, no volume-weighted averages were used.

Table 4. The mean ± std and the total OC and EC concentrations in rain water

ID	Mean ± std OC (ΣOC) (μg/mL)	Mean ± std EC (ΣEC) (μg/mL)
Rainfall-1	2.27 ± 2.20 (6.81)	< 0.15 μg/mL
Rainfall -2	2.79 ± 1.91 (13.9)	< 0.15 μg/mL
Rainfall -3*	-	-
Rainfall -4	2.18 ± 0.63 (11.0)	0.55 ± 0.40 (1.64)
Rainfall -5	2.73 ± 1.05 (27.3)	0.124 ± 0.076 (0.75)
Rainfall -6	3.28 ± 1.47 (19.7)	0.166 ± 0.20 (1.02)
Rainfall -7	2.40 ± 1.61 (28.8)	0.164 ± 0.25 (1.48)
Rainfall -8	4.23 ± 2.93 (64.6)	0.854 ± 0.995 (9.90)

*OC and EC were not measured.

std: standard deviation.

Measured EC values in the first two rainfall events were below the method detection limit (MDL) due to limited volumes of samples (1.0 mL) used to spike the 1.5 cm^2 filter punches. Again the measured mean EC levels corresponding to rainfall events 5, 6, and 7 were very close to MDL levels, while the EC concentrations measured in the sequential samples of 4th and 8th rainfall events were at higher levels which indicated the presence of combustion sources. The presence of EC in the samples can give valuable information about the pollution source since OC has varying numbers of primary and secondary sources but EC originates only from combustion sources and is a primary pollutant. The SEM-EDS analyses showed that the amounts of OC in the samples were contributed significantly by the primary biological aerosol particles (PBAPs) and biological organisms in this study. The observed high total OK concentrations (Table 4) clearly indicate the presence of PBAPs in the samples. This observation shows that the atmospheric coarse and total suspended particulate (TSP) samples collected directly on filter media can contain important amounts of biogenic particulates which might cause erroneous results in the calculations of secondary organic carbon (SOC) and organic materials (OM) using the EC tracer method as also stated in literature (Edgerton et al. 2009). High levels of OC were measured from the rainfall events 1, 2, 5, 6, and 7 with a very low corresponding EC levels which indicate, probably, the presence of significant amounts of PBAPs and biological organisms. During SEM analyses we observed only a few PBAPs in the samples of rainfall events 4 and 8 compared to about a hundred PMs in 12 mm^2 filter surface. On the other hand, the PBAPs were as abundant as the other types of PMs like terrestrial PMs, fly ash, and microfibers in the samples of rainfall events 1, 2, and 5. Therefore, observing measurable amounts of OC with very low levels of EC together with high PBAPs abundance indicate that the rainfall events 1, 2, and 5 are mainly contributed by the biogenic emissions, while the rest of the rainfall samples seem to be contributed mainly by the anthropogenic sources.

Particle size distributions

One of the main purposes of this study was to show the possibility of measuring particle size distributions in rain sequences directly by using laser diffraction technique and relate them with the PMs observed in SEM-EDS results. As an example of particle size distributions in the sequences of rainfall events, the sixth rainfall event with six sequences was chosen as an example in order to limit the number of figures. Particle size distributions in the sequential samples of rainfall event 8, as an additional example, were presented in supplementary materials (Fig. S11). In this study, we showed that the particle size distributions in rain sequences can be determined successfully, as reported in our previous work (Bayramoğlu Karşı et al. 2018).

The particle size distribution (Fig. 3) in the first sequence of the sixth rainfall event showed a 3 modal distribution with a dominant peak at about 2.0 μm with a volume density of about 10 % (primary y-axis of the graph). The second, fourth, and sixth sequences showed continuous 4 modal distributions. The third sequence showed three modal distributions and the fifth sequence had bimodal distribution. In general, if there is stagnant air during precipitation, in words if there is no new front from different sectors carrying rain, then the first two or three sequences show multimodal particle size distributions having higher volume densities at the coarse end of the particle distribution and the following sequences with a single peak centered at about 1.0 μm (Bayramoğlu Karşı et al. 2018). One of the most widely observed problems in the particle size distributions is the artifact peak at about 40-500 μm range, known as air bubble peak that can occur in aqueous dispersions. Fortunately, the presence of an air bubble peak can be recognized easily as follow: (1) if there is an air bubble peak then there should be a clear demarcation between the bubble peak and the sample particle peak, and (2) a microscopic check can clarify the presence of particles in the suspected size ranges. In addition to air bubble peaks, there are other possible ghost or artifact peaks like thermal, reflective, and optical modal artifacts. We did not observe any significant air bubble peak, an isolated peak, in this study as shown in Fig. 3, and the presence of sample peaks at the suspected regions of the particle size distribution was verified by measuring the particle sizes in the SEM images.

The number of peaks or multimodal distributions in particle sizes clearly showed the contributions caused by the washout, in which raindrops scavenge the PMs corresponding to the below cloud levels, and the rainout mechanisms. On the other hand, a sequence with a single peak centered at about 1.0 or 1.5 μm showed mainly the effect of the rainout process in the observed particle population.

The first sequence of the rainfall event given in Fig. 3 shows lower relative volume densities for the coarse particles than the expected amounts due to the uncollected rain event which prewashed the local atmosphere about 4 hours ago.

The median, Dv(50), value for the corresponding rainfall event changed between 1.39 μm (sequence 6) and 2.89 μm (sequence 2) means that half of the particulate matter sizes lie below this central value and the other half of particles lie above the central value. Particle sizes corresponding to Dv(10) showed that 10 % of the particle population lies below the corresponding particle sizes. Similarly, Dv(90) means that 90 % of the distribution lies below the value corresponding to Dv(90) in Fig. 3. Therefore, for the first sequence, half of the particulates have sizes higher and lower than 2.22 μm Dv(50), and 90 % of the particle population have sizes lower than 10.2 μm.

SEM-EDS results

SEM images and the morphologies of some selected primary biological aerosol particles (PBAPs) and biological organisms observed in the rainfall events sequences are presented in **Fig. 4** and **Fig. S1**. PBAPs were observed in almost all of the sequences but with dominant fractions in the first two or three sequences.

PBAPs are airborne biological PMs such as bacteria, pollen, fungal spores, and algae that are found in a widespread manner in the atmosphere (Delgado et al. 2010; W Li et al. 2020; Zeb et al. 2018). They are transported from the primary biological emission sources to the atmosphere (Delgado et al. 2010; Smith et al. 2018) and they play an important role in atmospheric chemistry, clouds, and the climate (W. Li et al., 2020). Additionally, abundances of PBAPs on the samples may lead to significant changes in OC/EC ratios which are widely used for source apportionments and secondary organic carbon determinations. Most of the PBAPs presented in **Fig. 4** and **Fig. S1** were obtained from the sequences of rainfall events 1 (September 20, 2019) and 8 (June 15, 2020).

The SEM-EDS results of the selected PMs were grouped with their corresponding sequence numbers in order to discriminate between the washout and rainout mechanisms. Because earlier sequences contain more earth crust materials, local pollutants, and PBAPs due to the washout process which scavenges PMs in a column of atmosphere from ground level to the clouds. SEM images, morphologies, and the sizes of PMs with the corresponding sequence numbers and the percent atomic abundances embedded as textboxes into the original images, were presented in the following figures. The PMs observed in the first two or three fractions of rainfall events are generally large in sizes and irregularly shaped particles together with primary biological aerosol particles (PBAPs) and submicron PMs. Therefore, the high population of these particles sometimes limits the number of targeted micron and submicron size single PMs. However, in contrast to samples of particulate matter on filter media collected directly from the atmosphere, there is an opportunity to have less population of large particles on the filter samples of rain sequences. In sequential rain samples, sequence volume can be divided into several fractional volumes, filtered, and prepared for the SEM EDS analyses to have more isolated single PMs. In the following figures, the selected PMs were grouped according to their appearances in rainfall sequences. Then the characterization and the probable sources of PMs were discussed with respect to backtrajectory calculations and the wind rose plots.

Some selected SEM images and the corresponding EDS results embedded into the original images of PMs observed from the first sequences of rainfall events 5 and 8 were presented in **Fig. S2** and **Fig. S3**. Back trajectories and the corresponding local wind rose plots for the rainfall events 5 and 8 were presented in **Fig S4 (a)** and **(b)**. Upper atmospheric backtrajectories and the local wind rose plots showed almost similar air-mass transport sectors. 1000 and 500 m air masses corresponding to the rainfall event 5 originate from the north and follow the path at about 1000-1500 m and then sink to the ground when they enter Turkey. The air masses spend about 25% of their residence time at ground level and reach the receptor site. However, 1500 m air mass originates from the western Mediterranean Sea and enters Turkey from the Aegean region, and follows the path starting from Marmara Region to the receptor site at an altitude of about 1000 m. Therefore, all the air masses pass over the zone involving iron-steel and power plant facilities (**Fig. S4**). On the other hand, 500, 1000, and 1500 m upper atmospheric backtrajectories corresponding to rainfall event 8 start from around Greece then enters Turkey from the west sector and then arrive at the receptor site from the eastern (500 and 1000 m) and north-western sectors (1500 m). Therefore, it is clear that both of the rainfall events were affected by emissions of iron-steel works and thermal power plants (Rainfall event 5 from Ereğli Iron-steel Facility and power plants,

Rainfall event 8 from Karabük Iron-steel Facility). Besides, the air masses of rainfall event 8 spent about 70 % (80 hours) of their total residence times (120 hours) at ground levels which can explain the observed PMs representing the emissions from forests and Karabük Iron Steel Facility (**Fig. S2** and **Fig. S3**). Two fly ash spherules **(a)**, irregularly shaped two sulfurous PMs and an iron-rich PM **(d)**, and a pyrite (FeS_2) **(e)** in **Fig. S2** were observed in the first sequential sample of rainfall event 8. The corresponding EDS results showed that rainfall event 8 had been affected by the emissions of both iron-steel works (natural iron ore, pyrite) and the thermal power plants (sulfur-rich fly ash PMs). The SEM images labeled as **(b)**, **(c)**, and **(f)** in **Fig. S2** showed that the rainfall event 5 had been affected mainly by the natural sources such as earth crust materials **(c)** and biological PMs **(b)** and organisms **(f)**. Some of the observed PMs in the first sequence samples of rainfall events 1 and 7 were given in **Fig. S3**. High abundances of PBAPs and crustal materials were observed in the samples of rainfall event 1 (**Fig. S3 (a)**, since the air mass of 1500 m corresponding to the event (**Fig. 2**) spent most of its residence time (about 60 %) at ground levels, between Zonguldak and Bartın coastal region. The SEM images and the EDS results of PMs (**(b)-(f)**) in **Fig. S3** were observed in the first sequential sample of rainfall event 7. The air masses of rainfall event 7 come from the north (over the Black Sea), however, the 500 m air mass sinks to the ground at the region where the iron steel facility and the power plants were localized and stays at that level for about 15 hours and then rises back to 500 m level. Therefore, this path clearly indicated that the 500 m air mass had been mainly affected by the emissions of the iron-steel facility, as also supported by the observed iron oxide spherules in the SEM-EDS results presented in **Fig. S3 (b)** and **(d)**, and a trigonal pyramidal iron oxide PM **Fig. S3 (f)**. A spherical C-O containing PM which is a grain of pollen **(e)** and another C-O containing perfect spherule of an organic matter in **(f)** which might be a secondary organic particle or a combustion product.

Some selected SEM-EDS results of the PMs observed in the second sequences of rainfall events 8 (**Fig. S5 (a)-(b)**, 2, 5, and 7 (**Fig. S6**) were **presented in Fig. S5** and **Fig. S6.** SEM images and the EDS results of PMs observed in the second sequence of rainfall event 8 show that the local or urban atmosphere has also an important contribution to the PM compositions in addition to the industrial activities. The presence of soot particle agglomerates (**Fig. S5 (a)**), fungal spore (**Fig. S5 (c)**) and sulfurous fly ash PMs with spherical and irregular shapes support this local contribution. The PMs in **Fig. S6** were observed in the second sequences of rainfall events 2 (**(e)** and **(f)**), 5 (**(a)** and **(b)**), and 7 (**(c)** and **(d)**). Air masses of 500, 1000, and 1500 m for rainfall event 2 pass over the Zonguldak industrial region, but the 500 m air mass sinks to ground level again, as observed for rainfall event 7, at the iron-steel facility region before reaching the sampling point. The SEM-EDS results in **Fig. S6 (a)** and **(b)** correspond to PMs observed in the second sequential sample of the fifth rainfall event. One of the particles **(a)** had a spherical and the other had a fibrous shape. Both the particles are classified as fly ash PMs originating most probably from thermal power plants due to low iron but higher sulfur abundances. Two organic fibrous PMs (**Fig. S6 (c)** and **(d)** with aspect ratios of 17 and 21, respectively, were observed in the second sequence of the rainfall event 7. The last two PMs in **Fig. S6 (e)** and **(f)** were observed in the second sequential sample of the second rainfall event. These two PMs are local contaminants originating from urban traffic that is, typical re-suspended road dust PMs involving mixes of organic spherules, earth crust material, and traces of Ti, Cu, Zn, Br and W (Bayramoğlu Karşı et al. 2020).

For the representation of third sequential samples, a sequential sample of rainfall event 8 was selected and the SEM-EDS results were presented in **Fig. S7**. Again the presence of sulfur-rich and both sulfur and iron-rich PMs show the contributions of emissions from the iron-steel facility and the coal combustions at the source region.

The observed PMs in the fourth and the fifth sequential samples (rainfall events 2, 4, and 7 as examples) and their SEM-EDS results, and morphologies were given in **Fig. S8**. The air mass backtrajectories of these three rainfall events originate from the N-NW sector and follow the west sector after arriving in Turkey. The 500 m air mass of rainfall event 2 sinks to the ground level for about 15 hours and then rises back to 500 m at the receptor site. The local wind blew from the N-NE sector with a wind speed of 3.6-5.7 m/s during the event. Therefore, the effect of local sources, mainly the urban atmosphere, were observed to be more effective than the industrial emission sources such as iron-steel and power plants facilities for the second rainfall event. Air masses of rainfall event 4 originate at the W sector and reach the receptor site from the S-SW sector and the upper atmospheric air masses of event 7 originate from N and follow the same path through the sampling site. Their corresponding local wind sectors were from E-NE (2.1-3.6 m/s and NE and S-SW (0.51-2.1 m/s) for events 4 and 7, respectively. The PMs observed in the fourth and the fifth sequential samples of the rainfall event 2 (**Fig. S8 (b** contained predominantly local pollutants such as road dust particles, textile fibers, microplastics, unburnt coal particles or biochar PMs and organic spherules that might be soot particles or secondary organic PMs. The second PM in **(e)** is a sulfurous organic PM that might be a soot particle from the coal combustion.

SEM-EDS results and morphologies of PMs from the sixth, seventh, and eighth sequential samples of rainfall event 7 were examined as examples and presented in **Fig. S9.** These sequential samples, again contained mainly local pollutants such as microplastics, microplastic-fibers contaminated with road dust particles, silicon dioxide and fly ash spherules, and spherical soot particles most probably from the urban traffic.

From the sequential samples (9th to 12th fractional samples) of rainfall event 7, we observed four types of particulates, namely, fibrous particulate **(a)**, spherical particulates **(a)**, **(b)**, **(d)**, and **(e)**, and flocculent particle **(c)**, and a fragmental particle **(f)** (**Fig. S10**). The identified PMs were an oval-shaped organic particle (most probably a pollen grain) and a mineral fiber of Si-Mg-Ca-Fe **(a)**, fly ashes **(b)**, **(d)**, and **(e)**, biochar or charcoal fragment (Ottosen et al., 2005; Peresani et al., 2018) combined with vegetative detritus **(c)**, and a biopolymer/chitin fragment **(f)**.

Results of this study showed that sequential sampling campaigns should be carried out at remote or at least rural sites in order to apportion the sources and the source regions of individual PMs successfully. Because the PM contributions from the local urban atmosphere and the other nearby point sources create challenges in the discrimination of the PMs with respect to their potential sources. However, it is clear that the sequential rainfall samples combined with particle size analyzer and SEM EDS are more advantageous in characterization and source apportionment of coarse and fine (> 0.1 μm) single particulate matter than routinely used sampling and analyses techniques.

Conclusions

This study showed that the source apportionment of single atmospheric PMs in sequential rain samples can be realized successfully when the SEM EDS analyses, particle size analyzer, and the chemical analyses results were combined. We showed that the particle size analyzer can directly be used successfully to determine the particle size distributions in the sequences of rainfall samples. The most frequently observed PMs, in this study, were primary biological aerosol particles (PBAPs), biological organisms and/or biological debris, fly ash from iron-steel and power plant facilities, resuspended road dust PMs, fibers, and fragments of microplastics,

agglomerated and single organic spherules from traffic emissions. PBAPs and the earth crustal PMs were the most abundant ones in the earlier sequences (the first and the second sequences, in general) of the rainfall events. Fly ash with high contents of sulfur and iron were identified as the marker for the iron-steel facility emissions, while the fly ash enriched with sulfur only were classified as the markers of coal-fired power plants. Results of the study showed also that the source apportionment of water insoluble single PMs in sequential samples would be more successfully carried out at remote or rural sites since the local sources (urban atmosphere in this study) obscure some of the PMs originating from regional or remote pollution sources.

Declarations

Declarations:

-Ethical Approval: Not applicable

-Consent to Participate: Not applicable

-Consent to Publish: Not applicable

-Authors Contributions:

Ercan Berberler: Investigation, Methodology, Supervision, Validation, Writing - original draft. Betül Tuba Gemici: Investigation, Methodology, Validation. Handan Ucun Özel: Conceptualization, Funding acquisition, Project administration, Resources, Writing - original draft, Writing – review & editing. Tuğçe Demir: Investigation. Duran Karakaş: Conceptualization, Supervision, Validation, Data curation, Resources, Writing – original draft, Writing – review & editing.

-Competing Interests: The authors have no conflicts of interest to declare that are relevant to the content of this article.

-Availability of data and materials: The datasets used and/or analyzed during the current study are available from the corresponding author on reasonable request. All data generated or analyzed during this study are included in this published article.

Supplementary data

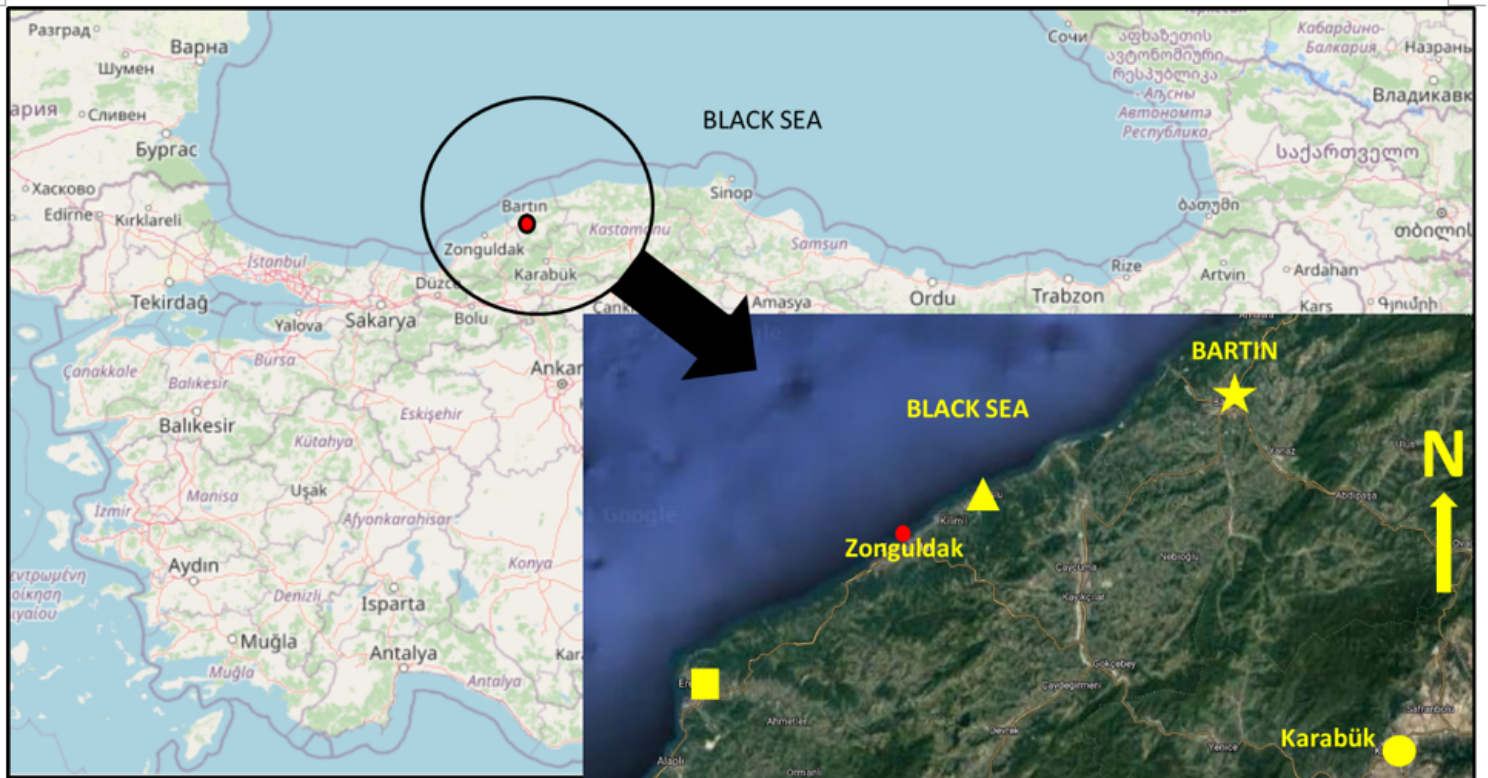Data was given in detail in supporting information.

References

Akoto O. Darko G, Nkansah MA (2011) Chemical composition of rainwater over a mining area in Ghana. Int J Environ Res 5(4):847–854. https://doi.org/10.22059/ijer.2011.442

Anatolaki C, Tsitouridou R (2009) Relationship between acidity and ionic composition of wet precipitation. A two years study at an urban site. Thessaloniki Greece Atmos Res 92(1):100–113. https://doi.org/10.1016/j.atmosres.2008.09.008

Anil I, Alagha O, Blaisi NI, Mohamed IA, Barghouthi MH, Manzar MS (2019) Source identification of episodic rain pollutants by a new approach: Combining satellite observations and backward air mass trajectories. Aerosol Air Qual Res 19(12):2827–2843. https://doi.org/10.4209/aaqr.2019.04.0187

Bayramoğlu Karşı MB, Berberler E, Berberler T, Aslan Ö, Yenisoy-Karakaş S, Karakaş D (2020) Correction and source apportionment of vehicle emission factors obtained from Bolu Mountain Highway Tunnel, Turkey. Atmos Pollut Res 11(12):2133–2141. https://doi.org/10.1016/j.apr.2020.06.021

Bayramoğlu Karşı MB, Yenìsoy-Karakaş S, Karakaş D (2018) Investigation of washout and rainout processes in sequential rain samples. Atmos Environ 190:53–64. https://doi.org/10.1016/j.atmosenv.2018.07.018

Bharti SK, Kumar D, Anand S, Poonam Barman SC, Kumar N (2017) Characterization and morphological analysis of individual aerosol of PM10 in urban area of Lucknow, India. Micron 103:90–98. https://doi.org/10.1016/j.micron.2017.09.004

Cvetković Ž, Logar M, Rosić A, Ćirić A (2012) Mineral composition of the airborne particles in the coal dust and fly ash of the Kolubara basin (Serbia). Periodico Mineral 81(2):205–223. https://doi.org/10.2451/2012PM0012

Delgado JD, García O E, Díaz AM, Díaz JP, Expósito FJ, Cuevas E, Querol X, Alastuey A, Castillo S (2010) Origin and SEM analysis of aerosols in the high mountain of Tenerife (Canary Islands). Nat Sci 02(10):1119–1129. https://doi.org/10.4236/ns.2010.210139

Ding J, Li J, Sun C, Jiang F, Ju P, Qu L, Zheng Y, He C (2019) Detection of microplastics in local marine organisms using a multi-technology system. Anal Methods 11(1):78–87. https://doi.org/10.1039/c8ay01974f

Ding X, Qi J, Meng X (2019) Characteristics and sources of organic carbon in coastal and marine atmospheric particulates over East China. AtmosRes 228:281–291. https://doi.org/10.1016/j.atmosres.2019.06.015

Edgerton ES, Casuccio GS, Saylor RD, Lersch TL, Hartsell BE, Jansen JJ, Hansen DA (2009) Measurements of OC and EC in coarse particulate matter in the southeastern United States. J Air Waste Manag Assoc 59(1):78–90. https://doi.org/10.3155/1047-3289.59.1.78

Garc S, Pe RM, Herrero C, Losada M (2002) Organic acids and aldehydes in rainwater in a northwest region of Spain. Atmos Environ 36:5277–5288

Garcia-Alcega S, Nasir ZA, Cipullo S, Ferguson R, Yan C, Whitby C, Dumbrell AJ, Drew G, Colbeck I, Tyrre S, Coulon F (2020) Fingerprinting ambient air to understand bioaerosol profiles in three different environments in the south east of England. Sci Total Environ 719:137542. https://doi.org/10.1016/j.scitotenv.2020.137542

Karaca F, Anil I, Yildiz A (2019) Physicochemical and morphological characterization of atmospheric coarse particles by SEM/EDS in new urban central districts of a megacity. Environ Sci Pollut Res 26(23):24020–24033. https://doi.org/10.1007/s11356-019-05762-2

Li CY, Ding M, Yang Y, Zhang P, Li Y, Wang Y, Huang L, Yang P, Wang M, Sha X, Xu Y, Guo C, Shan Z (2016) Portrait and Classification of Individual Haze Particulates. J Environ Prot 07(10):1355–1379. https://doi.org/10.4236/jep.2016.710118

Li W, Liu L, Xu L, Zhang J, Yuan Q, Ding X, Hu W, Fu P, Zhang D (2020) Overview of primary biological aerosol particles from a Chinese boreal forest: Insight into morphology, size, and mixing state at microscopic scale. Sci Total Environ 719:37520. https://doi.org/10.1016/j.scitotenv.2020.137520

Lim B, Jickells TD, Davies TD (1991) Sequential sampling of particles, major ions and total trace metals in wet deposition. Atmos Environ Part A General Topics 25(3–4):745–762. https://doi.org/10.1016/0960-1686(91)90073-G

Malli Mohan GB, Stricker MC, Venkateswaran K (2019) Microscopic Characterization of Biological and Inert Particles Associated with Spacecraft Assembly Cleanroom. Sci Rep 9(1):1–13. https://doi.org/10.1038/s41598-019-50782-0

Margiotta S, Lettino A, Speranza A, Summa V (2015) PM1 geochemical and mineralogical characterization using SEM-EDX to identify particle origin - Agri Valley pilot area (Basilicata, southern Italy). Nat Hazards Earth Syst Sci 15(7):1551–1561. https://doi.org/10.5194/nhess-15-1551-2015

Miler M, Gosar M (2013) Assessment of metal pollution sources by SEM/EDS analysis of solid particles in snow: A case study of Žerjav, Slovenia. Microsc Microanal 19(6):1606–1619. https://doi.org/10.1017/S1431927613013202

Ottosen LM, Pedersen AJ, Christensen IV (2005) Characterization of residues from thermal treatment of treated wood and extraction of Cu, Cr, As and Zn. Wood Sci Technol 39(2):87–98. https://doi.org/10.1007/s00226-004-0270-4

Peresani M, Ravazzi C, Pini R, Margaritora D, Cocilova A, Delpiano D, Bertola S, Castellano L, Fogliazza F, Martino G, Nicosia C, Simon P (2018) Human settlement and vegetation-climate relationships in the Greenland Stadial 5 at the Piovesello site (Northern Apennines, Italy). Quat Res (United States) 90(3):503–528. https://doi.org/10.1017/qua.2018.76

Pivokonsky M, Cermakova L, Novotna K, Peer P, Cajthaml T, Janda V (2018) Occurrence of microplastics in raw and treated drinking water. Sci Tot Environ 643:1644–1651. https://doi.org/10.1016/j.scitotenv.2018.08.102

Reisser J, Shaw J, Hallegraeff G, Proietti M, Barnes DKA, Thums M, Wilcox C, Hardesty BD, Pattiaratchi C (2014) Millimeter-sized marine plastics: A new pelagic habitat for microorganisms and invertebrates. PLoS ONE 9(6). https://doi.org/10.1371/journal.pone.0100289

Renard JB, Dulac F, Berthet G, Lurton T, Vignelles D, Jégou F, Tonnelier T, Jeannot M, Couté B, Akiki R, Verdier N, Mallet M, Gensdarmes F, Charpentier P, Mesmin S, Duverger V, Dupont JC, Elias T, Crenn V, … Daugeron D (2016) LOAC: A small aerosol optical counter/sizer for ground-based and balloon measurements of the size distribution and nature of atmospheric particles-Part 1: Principle of measurements and instrument evaluation. Atmos Meas Tech 9(4):1721–1742. https://doi.org/10.5194/amt-9-1721-2016

Rolph G, Stein A, Stunder B (2017) Real-time Environmental Applications and Display sYstem: READY. Environ Model Softw 95:210–228. https://doi.org/10.1016/j.envsoft.2017.06.025

Satsangi PG, Yadav S (2014) Characterization of PM2.5 by X-ray diffraction and scanning electron microscopy-energy dispersive spectrometer: Its relation with different pollution sources. Int J Environ Sci Technol 11(1):217–232. https://doi.org/10.1007/s13762-012-0173-0

Smith DJ, Ravichandar JD, Jain S, Griffin DW, Yu H, Tan Q, Thissen J, Lusby T, Nicoll P, Shedle S, Martinez P, Osorio A, Lechniak J, Choi S, Sabino K, Iverson K, Chan L, Jaing C, McGrath J (2018) Airborne bacteria in earth's lower stratosphere resemble taxa detected in the troposphere: Results from a new NASA Aircraft Bioaerosol Collector (ABC). Front Microbiol 9:1–20. https://doi.org/10.3389/fmicb.2018.01752

Stein AF, Draxler RR, Rolph GD, Stunder BJB, Cohen MD, Ngan F (2015) Noaa's hysplit atmospheric transport and dispersion modeling system. Bull Am Meteorol Soc 96(12):2059–2077. https://doi.org/10.1175/BAMS-D-14-00110.1

Wagner J, Wang ZM, Ghosal S, Wall S (2019) Source identification on high PM2.5 days using SEM/EDS, XRF, raman, and windblown dust modeling. Aerosol Air Qual Res 19(11):2518–2530. https://doi.org/10.4209/aaqr.2019.05.0276

Wang B, Harder TH, Kelly ST, Piens DS, China S, Kovarik L, Keiluweit M, Arey BW, Gilles MK, Laskin A (2016) Airborne soil organic particles generated by precipitation. Nat Geosci 9(6):433–437. https://doi.org/10.1038/ngeo2705

White EM, Landis MS, Keeler GJ, Barres JA (2013) Investigation of mercury wet deposition physicochemistry in the Ohio River Valley through automated sequential sampling. Sci Tot Environ 448:107–119. https://doi.org/10.1016/j.scitotenv.2012.12.046

Xhoffer C, Bernard P, Van Grieken R, Van der Auwera L (1991) Chemical Characterization and Source Apportionment of Individual Aerosol Particles over the North Sea and the English Channel Using Multivariate Techniques. Environ Sci Technol 25(8):1470–1478. https://doi.org/10.1021/es00020a017

Xia W, Rao Q, Deng X, Chen J, Xie P (2020) Rainfall is a significant environmental factor of microplastic pollution in inland waters. Sci Total Environ 732:139065. https://doi.org/10.1016/j.scitotenv.2020.139065

Xie RK, Seip HM, Liu L, Zhang DS (2009) Characterization of individual airborne particles in Taiyuan City, China. Air Qual Atmos Health 2(3):123–131. https://doi.org/10.1007/s11869-009-0039-x

Xue H, Liu G, Zhang H, Hu R, Wang X (2019) Elemental Composition, Morphology and Sources of Fine Particulates (PM2.5) in Hefei City, China. Aerosol Air Qual Res 19(8):1688–1696. https://doi.org/10.4209/aaqr.2018.09.0341

Yin C, Cheng X, Liu X, Zhao M (2020) Identification and classification of atmospheric particles based on SEM images using convolutional neural network with attention mechanism. Complexity. https://doi.org/10.1155/2020/9673724

Zeb B, Alam K, Sorooshian A, Blaschke T, Ahmad I, Shahid I (2018) On the morphology and composition of particulate matter in an urban environment. Aerosol Air Qual Res 18(6):1431–1447. https://doi.org/10.4209/aaqr.2017.09.0340

Figures

Figure 1

Location of the sampling site and important point sources. Star: Sampling site, Square: Ereğli Iron-steel Facility, Triangle: Çatalağzı Thermal Power Plant, Circle: Karabük Iron-steel Facility.
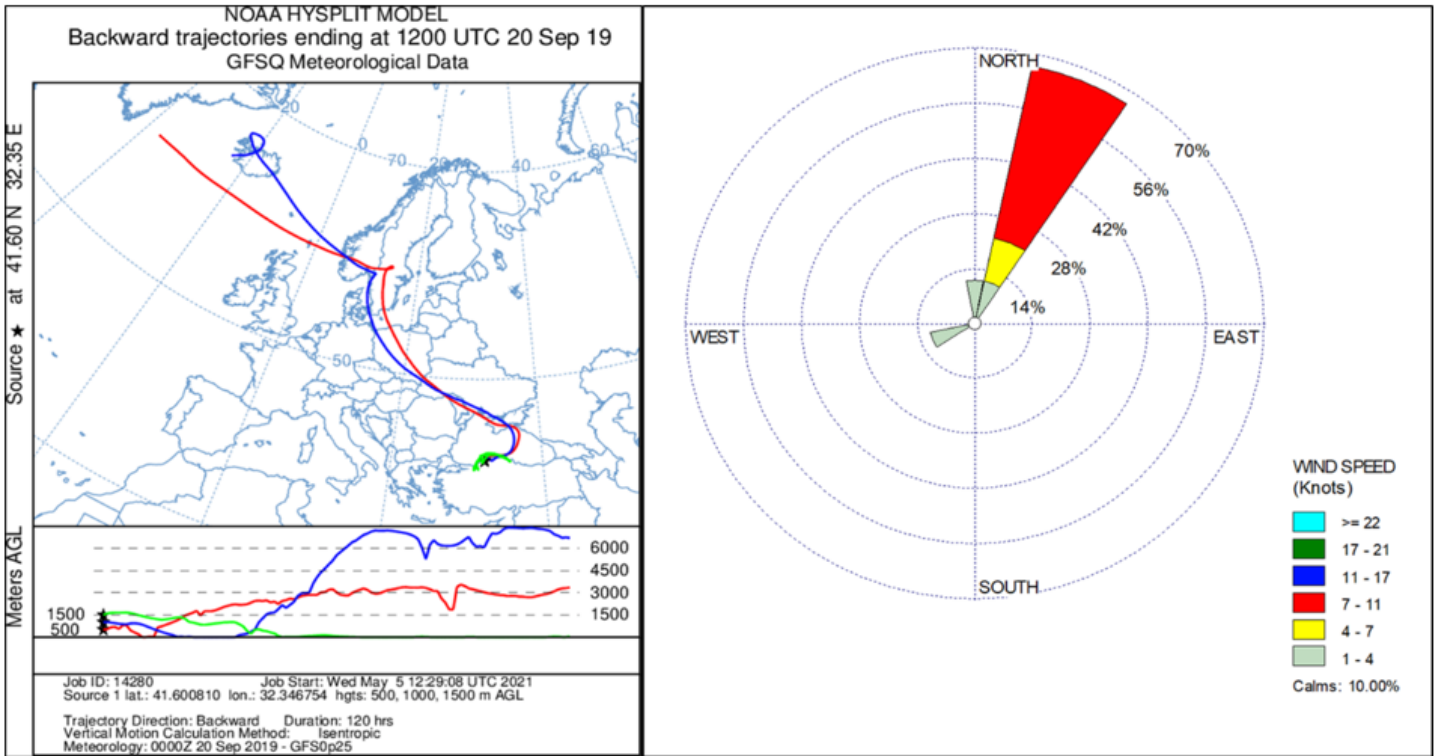
Figure 2

Five-day back trajectories at 500, 1000, and 1500 m (AGL) and local wind rose plot for the first rainfall event.
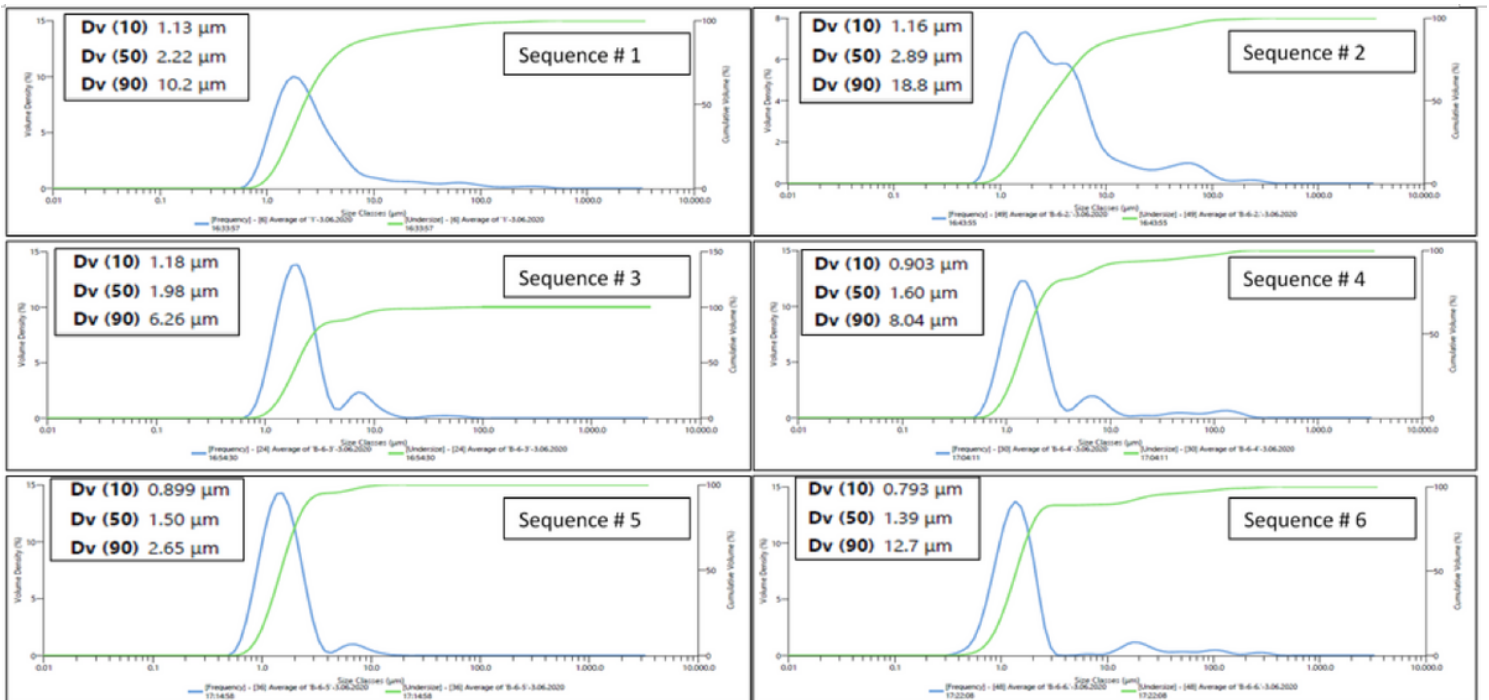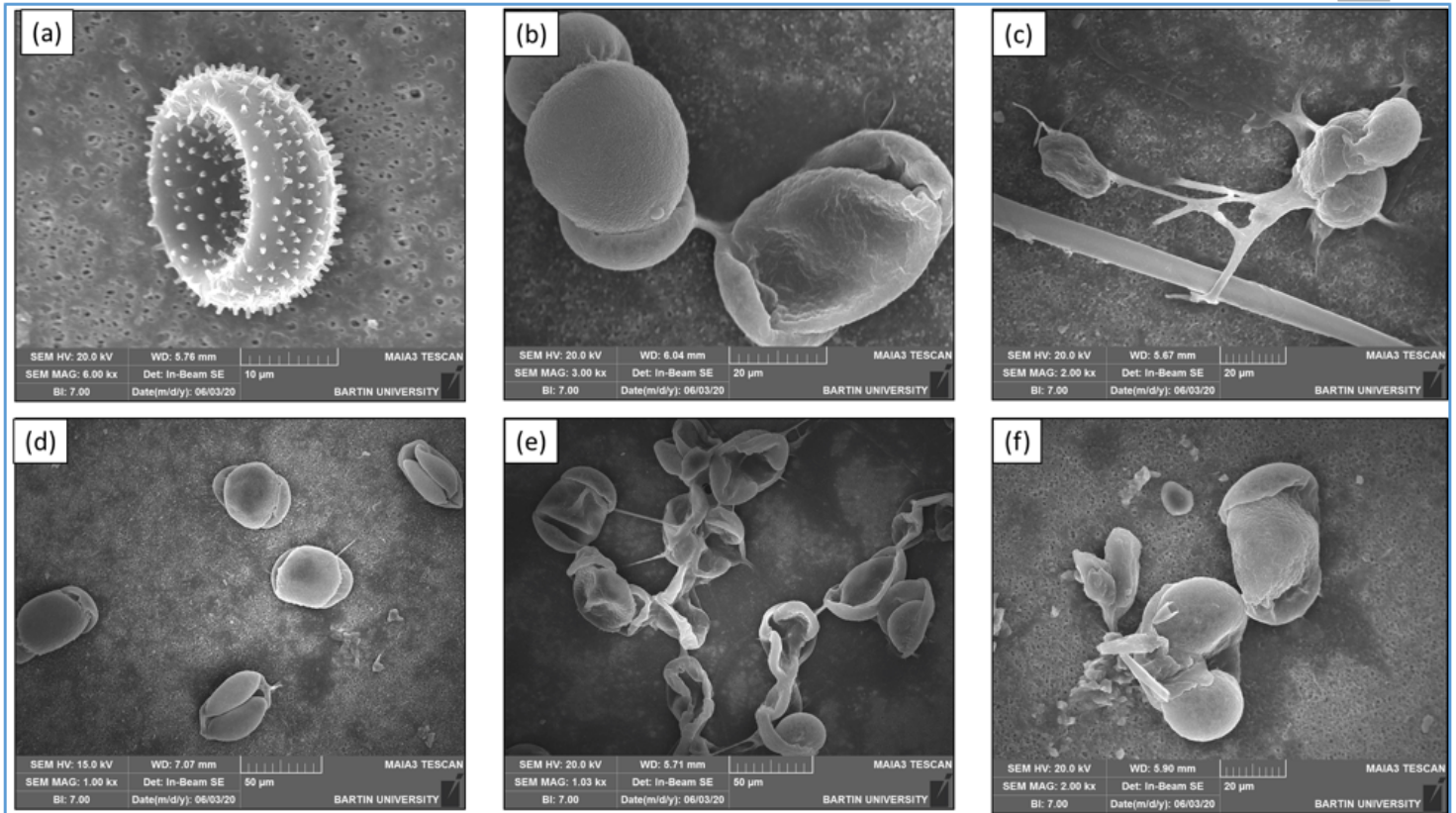

Figure 3

Particle size distributions in the sequences of the sixth rainfall event. The primary y-axis shows the percent volume densities (blue line) and the secondary y-axis shows the cumulative volume percentages (green line).

The embedded Dv(10), Dv(50), and Dv(90) values define the distribution widths on the x-axis. Dv(10) means 10 % of the particle population lies below the corresponding particle size. Dv(50) is the central point where half of the population lies below this value, and Dv(90) means 90 % of the particle population lies below the corresponding particle size.

Figure 4

SEM images of primary biogenic aerosol particles obtained from sequential samples of rainfall event 1. (a) centrally deformed spherical fungal spore with protuberances, (b)-(f) pollens, and pollen grains.

Supplementary Files

This is a list of supplementary files associated with this preprint. Click to download.

- Supplementarymaterials.docx